Spontaneous, stimulated, coherent and incoherent nonlinear wave mixing and Hyper-Rayleigh scattering; a unified quantum-field description

Oleksiy Roslyak & Shaul Mukamel

Department of Chemistry, University of California, Irvine, CA,92697

Abstract

By combining a quantum treatment of the radiation field with a superoperator formalism we present compact expressions for a broad variety of coherent and incoherent nonlinear optical signals. Spontaneous signals are classified according to the molecular coherence range: homodyne detected signals result from long range two particle coherence whereas Rayleigh and hyper-Rayleigh scattering are shown to be their short range counterparts. The dependence of the signals on wave vector, number of molecules and the molecular density is discussed for molecular and polymer solutes. Several two-photon induced techniques: second harmonic generation, hyper-Rayleigh scattering, two photon fluorescence and hyper-Raman are described within the same framework.

1 Introduction

Nonlinear optical signals are generated by the interaction of a material system with several laser beams. There are different types of signal classifications: spontaneous vs. stimulated, coherent vs. incoherent and short vs. long range. Some signals scale like $\sim N$ are others like $\sim N^2$ with the number of active molecules. The many types of signals are usually calculated using a variety of approaches, making it hard to establish their precise connections. The baffling plethora of non-linear techniques originate from varying numerous matter and field parameters (transition dipole moments, energy levels, carrier frequencies, pulse envelops, polarizations, delay times etc.). Esoteric acronyms (CARS, CSRS, HORSES etc.) further add to the confusion. Here we present a unified classification of these signals based on the last interaction that generates the signal field. This classification serves as a basis for a perturbative expansion, thus generating the various spectroscopic techniques.

Using a common approach the semiclassical theory of nonlinear spectroscopy which assumes a classical optical field interacting with a quantum matter has had a great success in describing coherent measurements [1, 2, 3, 4, 5, 6, 7, 8]. The signals are written in terms of response functions. The response functions which are obtained by a perturbative expansion of the polarization in the incoming fields. The polarization serves as a source in Maxwell's equations and generates the signal mode electric field. The perturbative expansion leads to various molecular pathways and the signal contains an interference between them. The fully quantum mechanical description of both optical field and matter developed here can treat both stimulated and spontaneous processes [7, 8, 9, 10, 11, 12]. Describing this formalism and its applications is the main subject of this presentation.

As an example we consider a set up where two beams of frequency ω_1 and ω_2 generate a signal with frequency $\sim \omega_1 + \omega_2$. Possible signals of this type are: sum frequency generation (SFG), hyper Raleigh scattering (HRS), two photon induced fluorescence (TPIF) and hyper Raman (HRA). These signals are used in various spectroscopic applications for probing molecular energy levels and ultrafast dynamical processes as well as in high resolution imaging and nonlinear microscopy. SFG, TPIF and HRS are commonly applied for biomolecular and cell imaging. Some studies had observed simultaneously two types of signals e.g. SFG+TPIF and SFG+HRS in the same system [9, 10].

The different types of nonlinear wave mixing signals are summarized in

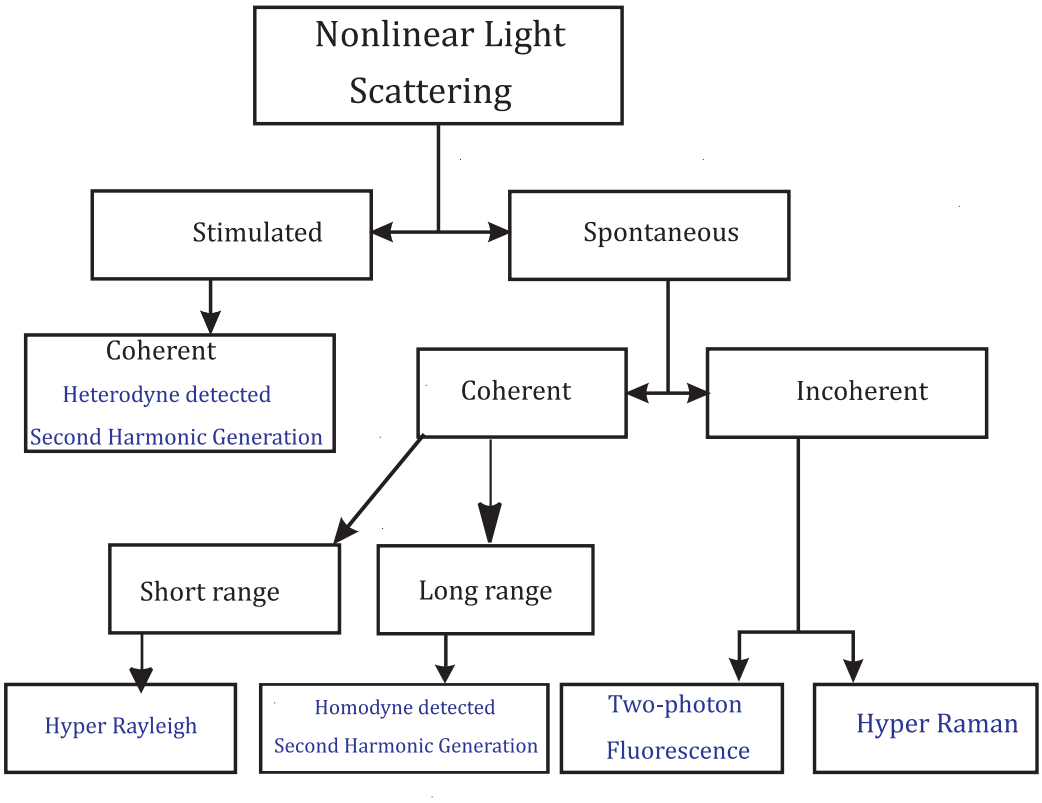

Figure 1: Classification of nonlinear wave mixing signals.

Fig. 1. The primary classification is into stimulated (coherent) $S_{ST,coh}$ and spontaneous S_{SP}. The latter are divided into incoherent $S_{SP,inc}$, coherent short range $S_{SP,coh,sr}$ and long range $S_{SP,coh,lr}$. This gives for the total signal:

$$S = S_{ST,coh} + S_{SP,inc} + S_{SP,coh,sr} + S_{SP,coh,lr} \tag{1}$$

The optical signals are broadly classified as either stimulated where the signal is generated in the direction of an existing strong classical field, or spontaneous where it is generated in a new direction i.e. the detected mode is initially in the vacuum state. The next layer of classification is into coherent, where the signal has a well defined phase with respect to the driving fields, or incoherent where no such phase relation exists. Stimulated signals are coherent, scale as $\sim N$ and the field itself (both amplitude and phase) can be measured by heterodyne detection. Spontaneous signals, in contrast, can be either coherent or incoherent. The homodyne detected coherent signal generated in a sample much larger than the optical wavelength is directional, and scales as $\sim N^2$. However short range correlations can induce a Rayleigh (hyper Rayleigh) scattering signal coming from pairs of closeby molecules. This signal is isotropic and scales as $\sim N$ [10] .

Spontaneous incoherent signals denoted spontaneous light emission (SLE) are generated by molecules which emit independently. They scale as $\sim N$ and may be further classified as either Raman (hyper Raman) or fluorescence.

The general classification shown in Fig. 1 holds to all orders in the fields. We shall recast the possible signals using compact superoperator expressions that can be expanded in the optical fields to generate specific signals. To first order we only have the coherent linear response which is self heterodyned, or ordinary Rayleigh scattering. The simplest model that shows all of these signals is depicted in Fig.2 where the emitted signals are either at or in the vicinity of $\omega_1 + \omega_2$. For this model the stimulated/coherent heterodyne detected signal is sum frequency generation (SFG). The spontaneous/coherent/long range signal is homodyne detected SFG. The spontaneous/coherent/short range signal is known in this case as hyper Rayleigh, and the spontaneous/incoherent signal is two-photon-induced light emission. The latter can further be classified as two-photon induced florescence and hyper Raman.

We next briefly introduce the two commonly used detection modes: heterodyne and homodyne. In the semiclassical approach to an $n + 1$ wave mixing measurement, n incoming waves interact with a molecule to induce

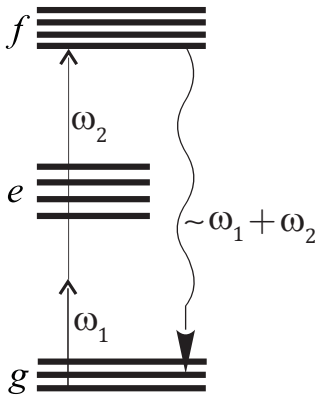

Figure 2: Level scheme for nonlinear two photon induced single photon emitted signals with frequencies in the vicinity of $\omega_1 + \omega_2$.

a polarization $\sim \langle V(\mathbf{r},t)\rangle_{\{n\}}$ (this notation will be explained in the next section). This polarization serves as a source in Maxwell's equations for the signal field $\mathcal{E}_{n+1}(\mathbf{r},t)$ [11]. The polarization must be further orientationally averaged and summed over all the molecules [3]. A more detailed analysis of the detection including propagation effects is given in Appendix A.

Heterodyne signals, detected by interference with a heterodyne mode, give both amplitude and phase of the nonlinear polarization. For a collection of N molecules, this is a coherent signal obtained by adding amplitudes from all molecules and is given by $\sim \Im N\langle V(\mathbf{r},t)\rangle_{\{n\}}\mathcal{E}^{\star}_{n+1}(\mathbf{r},t)$. Heterodyne signals are phase sensitive and directed along one of the possible 2^n phase matching directions $\Delta\mathbf{k} = \mathbf{k}_{\{n\}} - \mathbf{k}_{n+1} = 0$ $\mathbf{k}_{\{n\}} = \sum_{j=1}^{n} \pm\mathbf{k}_j$.

Homodyne detection is phase insensitive and only measures the intensity of the scattered light $\sim |\langle V(\mathbf{r},t)\rangle_{\{n\}}|^2$. It can be either incoherent or coherent. The former is a sum of individual molecular contributions $\sim N$, while the latter is produced by molecular pairs and scales as $\sim N(N-1)$. The coherence length is related to the optical phase variation between two molecules $\Delta\mathbf{k}(\mathbf{r}_\alpha - \mathbf{r}_\beta)$. For a sufficiently large $\Delta\mathbf{k}$ the phase oscillates rapidly and the coherent part of the signal vanishes. The coherent molecular response thus shows up in the phase-matching direction $\Delta\mathbf{k} = 0$ and depends quadratically $\sim N^2$ on the number of active molecules.

Inelastic processes, such as Hyper-Raman scattering are incoherent and do not produce a macroscopic electric field since different molecules emit

independently with random phases. One way to see this is by digressing from the semiclassical picture and looking at the joint state of the molecule and detected mode field ($|\texttt{mol,phot}\rangle$) at the end of the process: $|g,0\rangle + \alpha|g',1\rangle$ (See Fig. 2). This is a superposition of the initial state where the scattered mode is in the vacuum state with the molecule in state $|g\rangle$ and a state when the molecule is in the state $|g'\rangle$ with one emitted photon in the detected mode. The energy difference between the initial and final states of the molecule is supplied by the difference between the incoming and the signal modes (in Fig. 2 it corresponds to $\omega_1 + \omega_2 - \omega_s$). The expectation value of the signal field mode (formally defined in Eq.(3)) with this state vanishes since $|g\rangle$ and $|g'\rangle$ are orthogonal.

Parametric or elastic scattering processes are, in contrast, always phase matched $\Delta\mathbf{k} = 0$. The final state which now has the form $|g,0\rangle + \alpha|g,1\rangle$ does yield a finite field amplitude. At this level of theory Hyper-Rayleigh [12, 13, 14, 15] and Hyper-Raman [3, 16, 17, 10] scattering can be viewed as elastic and inelastic counterparts of two-photon induced fluorescence (i.e. incoherent and not phase matched).

The fully-microscopic description of the signals presented in the coming section treats both the molecules and the optical field quantum mechanically. This allows to classify the signals according to the initial state of the detected mode rather than by the detection method. If that mode initially contains a large number of photons one has a stimulated (emission or absorption), process. But if it is in the vacuum state we have a spontaneous process. Heterodyne detected signals are stimulated [11]. We shall mainly focus on spontaneous processes, but present the stimulated signals for completeness. Understanding the connection between the various signals is important for applications to such nonlinear imaging [18, 19]. We show that the coherent part of the scattering may be classified according to the coherence range. Rayleigh and nonlinear light scattering are coherent processes involving pairs of molecules. However they only probe short range correlations and therefore eventually scale as $\sim N$. The density dependent part of the Rayleigh signal is associated with intermolecular interactions. That component becomes dominant in the vicinity of anomalous first order phase transitions and vanishes for ordinary first order transitions in dilute solutions of molecules.

In the next section we calculate the signals using a quantum-mechanical description of the optical field and recast them into a form suitable for perturbative expansion that can be represented graphically close time path loop diagrams CTPL [20]. Some signals scale with the single-molecule and oth-

ers with molecular-pair distribution functions. The third section presents statistical models for these distribution functions. Signatures of structural phase transition are illustrated for a solution of weakly interacting molecules or polymers. The last section summarizes our results and presents a comparison of the various two-photon-induced signals associated with the level scheme in Fig. 2.

2 Spontaneous, stimulated, coherent and incoherent nonlinear wave mixing.

We start by partitioning the optical field into its positive and negative frequency components: $E(\mathbf{r},t)+E^{\dagger}(\mathbf{r},t)$. The positive frequency optical field at point $\mathbf{r}$ and time t is given by the operator:

$$E(\mathbf{r},t)=\sum_{j=1}^{n+1}\sqrt{\frac{2\pi\omega_j}{\Omega}}a_j(t)\exp\left(i\left(\mathbf{k}_j\mathbf{r}-\omega_j t\right)\right) \tag{2}$$

Here, $a_j\left(a_j^{\dagger}\right)$ is the annihilation (creation) operators for the j-the field mode, satisfying the bosonic commutation relation $\left[a_i,a_j^{\dagger}\right]=\delta_{i,j}$ and Ω is the quantization volume. The sum runs over all optical modes (including the detected, $n+1$, mode)

We take the origin of the coordinate at the center of the sample and assume a point detector located at $\mathbf{R}$. We define $E_{n+1}(\mathbf{R}+\mathbf{r},t)$ to be the field *generated* in the sample at point $\mathbf{r}$ and time t as seen by the detector:

$$E_{n+1}(\mathbf{R}+\mathbf{r},t)=\sqrt{\frac{2\pi\hbar\omega_{n+1}}{\Omega_{n+1}}}\times \tag{3}$$
$$\times a_{n+1}(t)\frac{\exp(i(\mathbf{k}_{n+1}(\mathbf{R}+\mathbf{r})-\omega_{n+1}t))}{|\mathbf{R}+\mathbf{r}|}$$

To eliminate the details of the detection geometry we define the plane wave signal mode in a local system of coordinates $E_{n+1}(\mathbf{r},t)$ by Eq.(2). For a detector far from the sample we have:

$$E_{n+1}(\mathbf{R}+\mathbf{r},t)\approx E_{n+1}(\mathbf{r},t)\times\frac{\exp(i(\mathbf{k}_{n+1}\mathbf{R}))}{|\mathbf{R}|}$$

Henceforth we assume that the signal mode is a plane wave. However we shall return to the spherical waves in the semiclassical treatment given in Appendix A. We shall calculate the field in the interaction picture (see e.g. Eq. (8)) where we eliminate its free propagation. Thus $E_{n+1}(\mathbf{r},t)$ defines the field *generated* at point $(\mathbf{r},t)$ in the sample. This field vanishes outside the sample.

We shall split the detected electric field as:

$$E_{n+1}(\mathbf{r},t) = \mathcal{E}_s(\mathbf{r},t) + E_s(\mathbf{r},t)$$

The classical (coherent) part $\mathcal{E}_s(\mathbf{r},t)$ is not affected by the interaction with matter, while the generated field $E_s(\mathbf{r},t)$ is initially ($t = -\infty$) in its vacuum state and changes its state due to the field/matter coupling. Following Ref. [21], the signal is defined as the change in the signal mode intensity due to the coupling with the system:

$$S(t) = S_{ST}(t) + S_{SP}(t) = \tag{4}$$
$$= \frac{\Omega}{2\pi\omega_s}\left[2\Re\int d\mathbf{r}\langle\mathcal{E}_s^\star(\mathbf{r},t)E_s(\mathbf{r},t)\rangle + \int d\mathbf{r}\langle E_s^\dagger(\mathbf{r},t)E_s(\mathbf{r},t)\rangle\right]$$

In order to calculate the expectation value of the optical field we now specify the total hamiltonian for the field and matter :

$$H(t) = H_0 + H_{int}(t) \tag{5}$$

Here H_0 describes the sample and H_{int} stands for its interaction with the optical modes. We assume that the sample is made of N identical molecules with the positions $\mathbf{r}_\alpha$, energy levels $\{|i\rangle\}$ and transition dipole moments $\mu_{i,j}$. We shall partition the dipole operator into the excitation $V^\dagger(\mathbf{r})$ and de-excitation $V(\mathbf{r})$ parts, where:

$$V(\mathbf{r}) = \sum_{\alpha=1}^{N}\delta(\mathbf{r}-\mathbf{r}_\alpha)\sum_j\sum_{k>j}\mu_{jk}|j\rangle\langle k| \tag{6}$$

Using Eq.(2) and Eq.(6), the radiation matter interaction in the Rotating Wave Approximation assumes the form:

$$H_{int}(t) = H_{int}^{(n+1)}(t) + H_{int}^{\{n\}}(t) = \tag{7}$$
$$= E_{n+1}(\mathbf{r},t)V^\dagger(\mathbf{r}) + E_{n+1}^\dagger(\mathbf{r},t)V(\mathbf{r}) +$$
$$+\sum_{j=1}^{n} E_j(\mathbf{r},t)V^\dagger(\mathbf{r}) + E_j^\dagger(\mathbf{r},t)V(\mathbf{r})$$

The two terms in Eq.(4) represent the stimulated and the spontaneous parts of the signals. These will be calculated by solving the Heisenberg equations of motion for the detected mode. The contribution from the points within the sample to the stimulated part is:

$$\frac{d}{dt}\langle \mathcal{E}_s^\star(\mathbf{r},t)E_s(\mathbf{r},t)\rangle = i\mathcal{E}_s^\star(\mathbf{r},t)\langle [H_{int},E_s(\mathbf{r},t)]\rangle = \tag{8}$$
$$= i\left(\frac{2\pi\omega_s}{\Omega}\right)\mathcal{E}_s^\star(\mathbf{r},t)\langle V(\mathbf{r},t)\rangle$$

Here we used the fact that the coherent part of the detected mode is not affected by the interaction with the molecules. $\langle\cdots\rangle$ denotes averaging over the radiation and matter degrees of freedom.

To proceed further we introduce superoperators which facilitate the bookkeeping of the various field/matter interactions [20]. For an arbitrary operator A these are defined as "Left" or "Right" type by their action on an operator X as:

$$A_L X = AX$$
$$A_R X = XA$$

We further define the transformed "Plus" and "Minus" superoperators:

$$A_- = \frac{1}{\sqrt{2}}\left(A_L - A_R\right)$$
$$A_+ = \frac{1}{\sqrt{2}}\left(A_L + A_R\right)$$

We shall recast Eq. (8) using the dipole superoperators:

$$\langle V(\mathbf{r},t)\rangle = \langle V_L(\mathbf{r},t)\rangle \equiv \mathtt{Tr}\left[V_L(\mathbf{r},t)\rho(t)\right] \tag{9}$$

The time evolution will be calculated in the interaction picture using the bare molecular Hamiltonian as a reference:

$$\langle V(\mathbf{r},t)\rangle = \langle \mathcal{T}V_L(\mathbf{r},t)\exp\left(-i\sqrt{2}\int_{-\infty}^{t}d\tau\int d\mathbf{r}' H_{int,-}(\tau,\mathbf{r}')\right)\rangle$$

Here $\sqrt{2}H_{int,-} = E_L V_L^\dagger + E_L^\dagger V_L - V_R^\dagger E_R - V_R E_R^\dagger$ and $\mathcal{T}$ is the time ordering operator in Liouville space which when acting on a product of the following

superoperators it rearranges them so that their time arguments increase from right to left.

Heterodyne detected $(n+1)$-wave mixing signals in a macroscopic ($N \gg 1$) sample are generated along one of the 2^n combinations of the n incoming wave vectors $\mathbf{k}_{\{n\}} = \pm\mathbf{k}_1 \pm \mathbf{k}_2 \cdots \pm \mathbf{k}_n$. This can be obtained by expanding Eq. (9) to first order in n incoming modes, each interacting once with a single molecule, and summing over all the molecules in the sample:

$$\langle V(\mathbf{r},t)\rangle_{\{n\}} = \sum_{\alpha=1}^{N} \delta\left(\mathbf{r}-\mathbf{r}_\alpha\right) \langle V_L(t)\rangle_{\{n\}} \mathsf{e}^{i\mathbf{k}_{\{n\}}\mathbf{r}} \tag{10}$$

The subscript $\{n\}$ signifies that the averaging is with respect to the density operator calculated by taking into account interactions of the incoming modes with a single molecule. The $n+1$ (signal) mode is treated separately.

When Eq.(8) together with the initial condition $\langle E_s(\mathbf{r}, t=-\infty)\rangle = 0$ and the expansion (10) are substituted into Eq.(4) we obtain the stimulated incoherent signal:

$$S_{ST}^{(n)}(t) = \mathtt{Im}\ F_1(\Delta\mathbf{k}) \int_{-\infty}^{t} d\tau \mathcal{E}_s^\star(\tau) \langle V_L(\tau)\rangle_{\{n\}} \tag{11}$$

The auxiliary function $F_1(\Delta\mathbf{k}) = \sum_\alpha \mathsf{e}^{i\Delta\mathbf{k}\mathbf{r}_\alpha}$ carries all information about the macroscopic sample geometry as well as the spatial distribution of molecules. It is responsible for phase matching, which is a hallmark of heterodyne detected signals. Self-heterodyne signals such as pump-probe [21, 11], and stimulated Raman/Hyper-Raman scattering also fall into the stimulated signal category.

We next turn to the spontaneous component of the signal (4). The contribution from point $\mathbf{r}$ within the sample to this component is obtained by solving the Heisenberg equation of motion:

$$\begin{aligned} \frac{d}{dt}\langle E_s^\dagger(\mathbf{r},t) E_s(\mathbf{r},t)\rangle &= i\langle\left[H_{int}, E_s^\dagger(\mathbf{r},t)E_s(\mathbf{r},t)\right]\rangle = \\ &= 2\Im\left(\frac{2\pi\omega_s}{\Omega}\right)\langle E_s^\dagger(\mathbf{r},t)V(\mathbf{r},t)\rangle \end{aligned} \tag{12}$$

with the initial condition $\langle E_s^\dagger E_s\rangle(t=-\infty) = 0$. The right hand side of this equation may be factorized into a field and matter parts provided the density

operator is treated perturbatively with respect to the E_s part of the signal mode.

To first order the spontaneous signal assumes the form:

$$S_{SP}^{(n)}(t) = 2\mathtt{Re}\int d\mathbf{r}\int d\mathbf{r}' e^{i\mathbf{k}_{n+1}(\mathbf{r}-\mathbf{r}')}\times \tag{13}$$
$$\times \int_{-\infty}^{t} d\tau \int_{-\infty}^{\tau} d\tau' e^{i\omega_{n+1}(\tau-\tau')}\langle \mathcal{T}V_L(\mathbf{r},\tau)V_R^{\dagger}(\mathbf{r}',\tau')\rangle_{\{n\}}$$

When all interactions with the optical fields occur with the same molecule $\langle \mathcal{T}V_L(\mathbf{r},\tau)V_R^{\dagger}(\mathbf{r}',\tau')\rangle_{\{n\}}$ assumes the form $\langle \mathcal{T}V_L(\mathbf{r},\tau)V_R^{\dagger}(\mathbf{r}',\tau')\rangle_{\{n\}}\delta\left(\mathbf{r}-\mathbf{r}'\right)$ and we recover the incoherent signal (13). Expanding it to first order in the interactions with each of the incoming modes we obtain:

$$S_{SP,incoh}^{(n)}(t) = 2\mathtt{Re}F_1(0)\int_{-\infty}^{t} d\tau \int_{-\infty}^{\tau} d\tau' \mathtt{e}^{i\omega_{n+1}(\tau-\tau')}\langle \mathcal{T}V_L(\tau)V_R^{\dagger}(\tau')\rangle_{\{n\}} \tag{14}$$

Incoherent ($F_1(0) = N$) homodyne detected signals are phase insensitive. Examples are n photon induced Fluorescence and Hyper-Raman scattering.

The coherent part of the spontaneous signal is obtained when the optical modes are allowed to interact with all possible molecular pairs in the sample. Interactions with different molecules are not time ordered and $\langle \mathcal{T}V_L(\mathbf{r},\tau)V_R^{\dagger}(\mathbf{r}',\tau')\rangle$ can be factorized into $\langle V_L(\mathbf{r},\tau)\rangle\langle V_R^{\dagger}(\mathbf{r}',\tau')\rangle$. By expanding the two factors to first order in each of the n incoming modes we obtain the coherent part of the homodyne detected signal:

$$S_{SP,coh}^{(n)}(t) = \mathtt{Re}\ F_2(\Delta\mathbf{k})|\int_{-\infty}^{t} d\tau e^{i\omega_{n+1}\tau}\langle V_L(\tau)\rangle_{\{n\}}|^2 \tag{15}$$

Here we have used the identity:

$$\int_{-\infty}^{t} d\tau \int_{-\infty}^{\tau} d\tau' = \frac{1}{2}\int_{-\infty}^{t} d\tau \int_{-\infty}^{t} d\tau'$$

The auxiliary function $F_2(\Delta\mathbf{k}) = \sum_{\alpha}\sum_{\beta\neq\alpha} e^{i\Delta\mathbf{k}(\mathbf{r}_\alpha-\mathbf{r}_\beta)}$ is determined by the distribution function of molecular pairs as well as the sample geometry. Eq. (15) describes for example n-harmonic generation and Hyper-Rayleigh scattering.

Eqs. (11), (14), (15) constitute the formal expressions for various signals. Specific signals will be calculated in Section 4. In the next section we focus on the molecular and molecular-pair distribution functions: $F_1(\Delta\mathbf{k})$ and $F_2(\Delta\mathbf{k})$.

3 $n+1$ wave mixing in fluids and polymer solutions; the role of molecular distribution functions.

We now examine more closely the role of molecular distributions in nonlinear wave scattering. Following Ref. [22] we shall consider a system of N identical hard sphere molecules in a solvent occupying the volume $L^3 \approx \Omega'$. The molecular diameter a is smaller than the wavelength λ_{n+1} of the detected mode. Eqs. (11), (14), (15) describe the scattering due to the solute. Three cases will be considered. First, we will look at the scattering from an ideal solute with no long range order as depicted in Fig. 3(c). Second we investigate the scattering from a solution of polymer molecules [23] (See Fig. 3(d)). Finally we discuss a real solution close to a phase transition point.

For large samples $L|\Delta\mathbf{k}| \gg 1$ the problem can be treated in the continuum limit, where Maxwell's equations self-consistently connect the polarization $\langle V(\mathbf{r},t)\rangle_{\{n\}}$ and the induced electric field $E_{n+1}(\mathbf{r},t)$. The signal is then calculated in two steps. First, the atoms act as the primary sources induce the field at the aperture [24]. This field serves as the secondary source and for the signal, which is calculated using the propagator formalism. In this limit both semiclassical and quantum approaches yield the same result as shown in Appendix A.

In the opposite limit $L|\Delta\mathbf{k}| \ll 1$ the phase factor $\Delta\mathbf{k}\cdot\mathbf{r}$ does not change appreciably within the sample and the sample can no longer be treated as a continuous medium. Statistical molecular properties then affect the signal.

3.1 Stimulated vs. Spontaneous incoherent signals.

Both signals described by Eqs. (11) and (14) are determined by the molecular distribution. The probability to find a solute molecule in the volume $d\mathbf{r}$ centered at $\mathbf{r}$ is given by $F_1(\mathbf{r})d\mathbf{r}/\Omega'$. The molecular distribution function is normalized so that its average value in the sample volume Ω' is the total

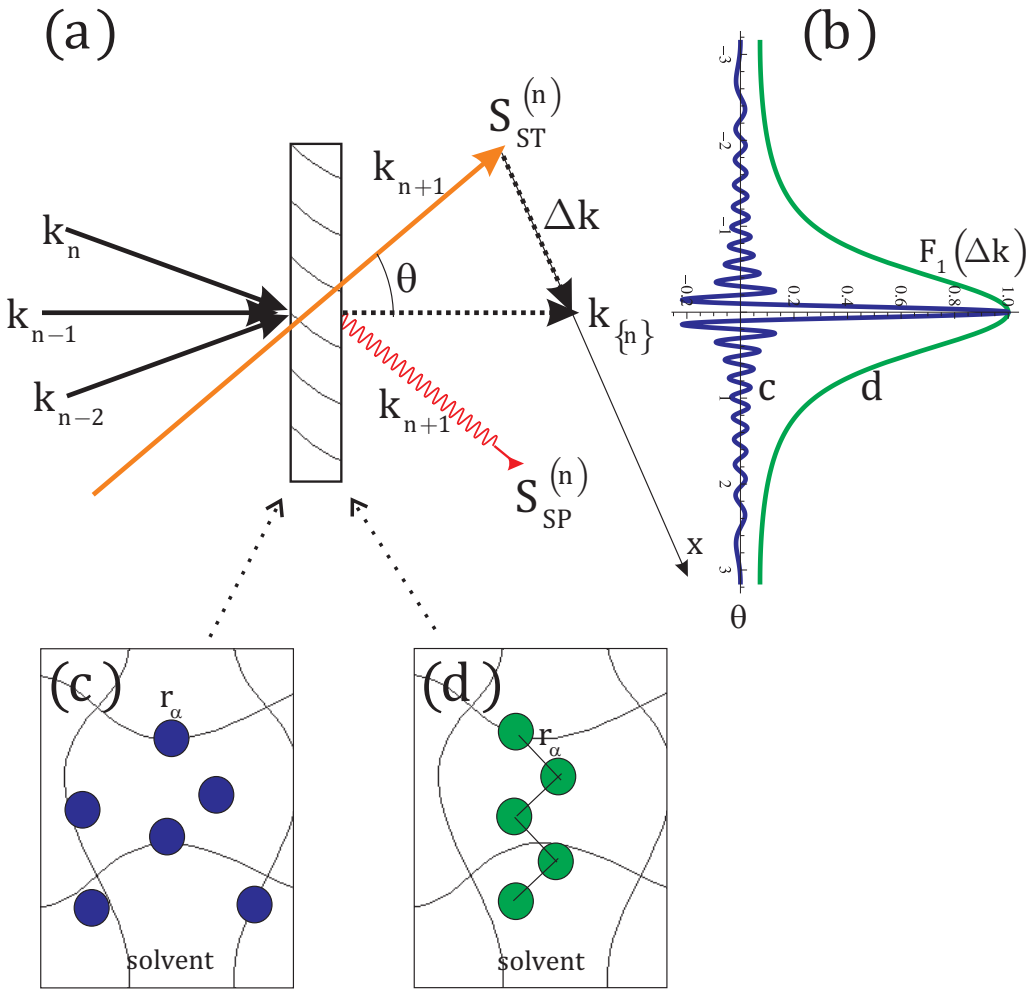

Figure 3: (a) schematic of nonlinear wave mixing. θ is the phase matching angle between stimulated (red thick line)/spontaneous (wavy line) and a linear combination of the incoming modes (doted line). (b) the angular distribution of the stimulated signal from an ideal solute of noninteracting (blue rapidly oscillating curve) and polymer solute (green smooth curve). The parameters used are: $L/\lambda = 10$, $N = 100$, $b = 0.01$. $F_1(\Delta k)$ is normalized to the number of molecules. (c) ideal solute. (d) polymer solute.

number of molecules: $(N/\Omega')\int_{\Omega'} F_1(\mathbf{r})d\mathbf{r} = N$. By converting the summation over a large number of independent molecular coordinates $\mathbf{r}_\alpha$ to an integration over $\mathbf{r}$ we obtain:

$$F_1(\Delta\mathbf{k}) = \frac{N}{\Omega'}\int_{\Omega'} F_1(\mathbf{r})e^{i\Delta\mathbf{k}\cdot\mathbf{r}}d\mathbf{r} \tag{16}$$

More generally, the molecular distribution function must also include internal molecular degrees of freedom and rotational averaging. These are neglected here.

3.1.1 Ideal solutions.

In the absence of long range order ($F_1(\mathbf{r}) = 1$, Fig.3(c). Assuming that $\Delta\mathbf{k}$ is in the $\hat{x}$ direction as shown in Fig.3(a), straightforward calculation of the integral (16) yields:

$$F_{1,fluid}(\Delta\mathbf{k}) = N\mathcal{P}_{fluid}(\theta) \tag{17}$$

with the polarization angular distribution:

$$\mathcal{P}_{fluid}(\theta) = \mathtt{sinc}(2\pi L\sin(\theta/2)/\lambda_{n+1})$$

Here λ is the wavelength; θ is the angle between detected $\mathbf{k}_{n+1}$ mode and the induced polarization given by a linear combination of the incoming modes $\mathbf{k}_{\{n\}}$.

3.1.2 A polymer solution.

The molecular probability distribution of polymers (Fig.3(d)) can be calculated using the theory of random walks [25]:

$$\frac{N}{\Omega'}F_1(\mathbf{r})d\mathbf{r} = \frac{2}{N}\sum_j\sum_{i>j} W_{i,j}(r)d\mathbf{r} \tag{18}$$

$$W_{i,j}(r) = \left(\frac{3}{2\pi b^2\left(|i-j|\right)}\right)^{3/2}\exp\left(\frac{-3r^2}{2b^2\left(|i-j|\right)}\right) \tag{19}$$

The walk step b depends on the polymer geometry. $W_{i,j}(r)d\mathbf{r}$ is the probability of finding j'th polymer unit at distance r from the i'th unit in the

volume element $d\mathbf{r}$. Converting the summation in Eq. (19) to an integration and substituting Eq. (18) in Eq. (16) we obtain:

$$F_{1,poly}(\Delta\mathbf{k}) = N\mathcal{P}_{poly}(\theta, N) \tag{20}$$
$$\mathcal{P}_{poly}(\theta, N) = \frac{2}{U(N,\theta)}\left[\mathsf{e}^{U(N,\theta)} - 1 + U(N,\theta)\right]$$
$$U(N,\theta) = \frac{8\pi^2}{3}\frac{b^2 N}{\lambda_{n+1}^2}\sin^2(\theta/2)$$

Eq. (11) together with Eq. (17) or (20) imply that the stimulated signal is peaked in the direction $\Delta\mathbf{k} = 0$. Long-range order now breaks the linear $\sim N$ dependence of the signal of ideal solutions.

3.2 Spontaneous coherent signals.

Spontaneous coherent signals given by Eq. (15) defined as the Fourier transform of the molecular pair distribution function:

$$F_2(\Delta\mathbf{k}) = \frac{N(N-1)}{2\Omega'^2}\int\!\!\int_{\Omega'} F_2(\mathbf{r}_\alpha, \mathbf{r}_\beta)\mathsf{e}^{i\Delta\mathbf{k}(\mathbf{r}_\alpha - \mathbf{r}_\beta)}d\mathbf{r}_\alpha d\mathbf{r}_\beta \tag{21}$$

Here $N(N-1)/2\Omega'^2 F_2(\mathbf{r}_\alpha, \mathbf{r}_\beta)d\mathbf{r}_\alpha\mathbf{r}_\beta$ is the joint probability of the molecules in the pair between $\mathbf{r}_\alpha, \mathbf{r}_\beta$ and $\mathbf{r}_\alpha + d\mathbf{r}_\alpha, \mathbf{r}_\beta + d\mathbf{r}_\beta$. The pair distribution function is normalized so that when integrated over the sample it gives the total number of molecular pairs:

$$\frac{N(N-1)}{2\Omega'^2}\int_{\Omega'}\int F_2(\mathbf{r}_\alpha, \mathbf{r}_\beta)d\mathbf{r}_\alpha d\mathbf{r}_\beta = \frac{N(N-1)}{2} \tag{22}$$

We shall partition F_2 as:

$$F_2(\mathbf{r}_\alpha, \mathbf{r}_\beta) = \lim_{|\mathbf{r}_{\alpha,\beta}|\to\infty} F_1(\mathbf{r}_\alpha)F_1(\mathbf{r}_\beta) + g_2(\mathbf{r}_\alpha, \mathbf{r}_\beta) \tag{23}$$

where $\mathbf{r}_{\alpha,\beta} = \mathbf{r}_\alpha - \mathbf{r}_\beta$. The function g_2 represents the deviation of $F_2(\mathbf{r}_\alpha, \mathbf{r}_\beta)$ from a product of single molecule distributions $F_1(\mathbf{r}_\alpha)F_1(\mathbf{r}_\beta)$ and is a measure of intermolecular interactions.

3.2.1 Long-range coherence.

The first term in Eq. (23) when substituted into Eq. (15) yields the long range coherent spontaneous signal with the molecular distribution function:

$$F_2(\Delta\mathbf{k}) = N(N-1)\mathcal{P}^2_{fluid}(\theta) \tag{24}$$

Note that for linear light scattering ($n = 1$), the signal (24) is indistinguishable from the incident beam. However the signal can be clearly resolved for nonlinear scattering with non-collinear beam geometry.

A similar result holds for a collection of N' polymers each made of N molecules. In the absence of long range order between the polymer molecules, one can use Eq. (24), with $N \to N'N$; (See the neglected first term in Eq. (11) of Ref. [25]).

3.2.2 Short-range coherence.

Short-range coherent spontaneous signals are given by Eq. (15). The distance between the molecules involved in the light-matter interaction is restricted by $g_2(\mathbf{r}_\alpha, \mathbf{r}_\beta)$, so that $r_{\alpha,\beta}/\lambda_{n+1} \ll 1$ and the exponential phase factor in Eq. (21) can be set to unity.

We start by considering a solution of hard sphere molecules of diameter a , the volume per solute molecule: $\pi a^3/6 = \Omega'/N = v$. In this case [26]:

$$g_2(\mathbf{r}_{\alpha,\beta}) = \begin{cases} 0, & r_{\alpha,\beta} > a \\ -1, & r_{\alpha,\beta} \leq a \end{cases} \tag{25}$$

Using the identity $\frac{1}{\Omega'} \int\int d\mathbf{r}_\alpha \mathbf{r}_\beta g_2(\mathbf{r}_\alpha, \mathbf{r}_\beta = \int d\mathbf{r}_{\alpha,\beta} g_2(r_{\alpha,\beta})$ we obtain:

$$F_{2,fluid}(\Delta\mathbf{k}) = -\frac{N-1}{2} \tag{26}$$

The short-range interaction for a collection of N' polymer molecules each comprised of N molecular segments has been calculated in Ref. [25]:

$$F_{2,poly}(\Delta\mathbf{k}) = \frac{N^4}{v'^2} X \mathcal{P}^2_{poly}(\theta, N) \tag{27}$$

where $v' = \Omega'/N'$ is the volume per single polymer molecule and X describes the average short range interaction between the segments of two polymer molecules. Note that the first term in Eq. (13 (a)) of Ref. [25] corresponds

to the extra-short range coherent signal from the collection of the thread-like polymer molecules $\sim \frac{NN'}{\Omega'} F_{1,poly}(\Delta\mathbf{k})$. The coherence length is limited to a single polymer molecule.

To discuss the validity of the hard sphere model (26) we impose certain limitations on the solute molecules and their interactions. The solute is treated as non-ideal gas of classical molecules capable of undergoing a thermodynamic phase transitions. Second, the pair interaction potential falls off with the fourth or higher power of the distance. Third, the total potential energy of the system is representable as the sum of pair potentials which only depends only on the distance.

The deviation of the solute from the ideal gas is described by the fugacity Z normalized in density v^{-1} units:

$$Z = v^{-1} \exp\left(-\sum_{l\geq 1} \beta_l v^{-l}\right) \tag{28}$$

The irreducible integrals β_l are defined so that for the ideal gas $\beta_l \to 0$. We rewrite Eq.(28) in its differential form:

$$\frac{\partial \ln Z}{\partial \ln v} = \sum_{l\geq 1} l\beta_l v^{-l} - 1 \tag{29}$$

The pressure of the gas P above the solvent also shows the deviation from the ideal gas, which can be formally written with irreducible integrals as:

$$\left(\tfrac{\partial P}{\partial Z}\right)_T = \frac{NkT}{Zv} \tag{30}$$

$$\left(\tfrac{\partial P}{\partial \Omega'}\right)_T = -\frac{NkT}{\Omega'^2}\left(1 - \sum_{l\geq 1} l\beta_l v^{-l}\right) \tag{31}$$

where k is the Boltzmann constant and T is the temperature. Using the generalized form of the grand partition function (28), as well as connection between the cluster and irreducible integrals, it has been shown [26, 27] that:

$$\frac{1}{2\Omega'} \int g_2(\mathbf{r}_{\alpha,\beta}) d\mathbf{r}_{\alpha,\beta} = -\frac{Z^2 v^2}{2kT\Omega'} \left(\frac{\partial^2 P}{\partial^2 Z}\right)_T \tag{32}$$

where P is the osmotic pressure. Substituting Eq.(30) into Eq.(32) and

utilizing Eq.(29) yields:

$$\frac{1}{2\Omega'}\int g_2(\mathbf{r}_{\alpha,\beta})d\mathbf{r}_{\alpha,\beta} = -\frac{v}{2\Omega'}\left(1-\frac{1}{1-\sum\limits_{l\geq 1} l\beta_l v^{-l}}\right) \tag{33}$$

Combining with Eqs. (23) and (21) we get:

$$F_{2,fluid}(\Delta\mathbf{k}) = -\frac{N-1}{2}\left(1-\frac{1}{1-\sum\limits_{l\geq 1} l\beta_l v^{-l}}\right) = \tag{34}$$

$$= -\frac{N-1}{2}\left[1-\frac{NkT}{\Omega'^2}\left(\frac{\partial P}{\partial \Omega'}\right)_T^{-1}\right]$$

This confirms that the short range coherent spontaneous signal vanishes in an ideal solution. It also suggests that short range coherent signals from the solute in the absence of strong Van-Der-Waals forces is not phase sensitive and depends on the solute density v^{-1}. It thus represents Rayleigh ($n = 1$) and Hyper-Rayleigh ($n > 1$) scattering.

The first-principles calculation of the irreducible integrals β_l is a challenging task [27]. We next discuss the role of $\sum l\beta_l v^{-l}$. Phase transitions are characterized by divergence of the fugacity density series (28) on the real axis at $T = T_c$. Hence, $\sum l\beta_l v^{-l}$ either diverges (first order transitions) or becomes unity (anomalous first order transitions) [28, 29]. In the first case, $\sum l\beta_l v^{-l}$ increases at the singularity and reaches unity at some temperature T_0 lower than the temperature at which the singularity moves into the complex plane T_c. Close to T_0 the slight change in the partial volume of the solute dos not change with pressure and the second term in Eq. (34) dominates the short range coherent spontaneous signal.

An anomalous first-order transition occurs in the temperature range $T_o < T_a < T_c$. One can then neglect the second term in Eq. (34) and the signal coincide with the hard spheres model (26). The $(N-1)/2$ factor signifies that only pairs of nearby molecules contribute to the short range coherence.

4 Application to two-photon-induced signals.

We have presented a unified microscopic description of $n+1$ wave mixing processes. The nonlinear signal defined as the change in the intensity of the

detected mode due to the other n optical modes is formally expressed in terms of polarization superoperators which are calculated by the Heisenberg equations of motion for the field (stimulated signals) or for the field intensity (spontaneous signals). We have identified four types of signals, and connected them to standard statistical quantities, namely the molecular and molecular pairs distribution functions. Our formal results can be summarized as follows:

$$S^{(n)}(t) = S^{(n)}_{ST}(t) + S^{(n)}_{SP,icoh}(t) + S^{(n)}_{SP,coh,lr}(t) + S^{(n)}_{SP,coh,sr}(t) \tag{35}$$

$$S^{(n)}_{ST}(t) = \mathtt{Im}\ N \left\{ \begin{array}{c} \mathcal{P}_{fluid}(\theta) \\ \mathcal{P}_{poly}(\theta, N) \end{array} \right\} \int_{-\infty}^{t} d\tau \mathcal{E}^{\star}_{s}(\tau) \langle V_L(\tau) \rangle_{\{n\}} \tag{36}$$

$$S^{(n)}_{SP,incoh}(t) = 2\mathtt{Re}\ N \int_{-\infty}^{t} d\tau \int_{-\infty}^{\tau} d\tau' \mathtt{e}^{i\omega_{n+1}(\tau-\tau')} \langle \mathcal{T} V_L(\tau) V^{\dagger}_R(\tau') \rangle_{\{n\}} \tag{37}$$

$$S^{(n)}_{SP,coh,lr}(t) = N(N-1)|\mathcal{P}_{fluid}(\theta) \int_{-\infty}^{t} d\tau e^{i\omega_{n+1}\tau} \langle V_L(\tau) \rangle_{\{n\}}|^2 \tag{38}$$

$$S^{(n)}_{SP,coh,sr}(t) = \left\{ \begin{array}{c} -\frac{N-1}{2}\mathtt{Re} \left(1 - \left(1 - \sum_{l \geq 1} l \beta_l v^{-l} \right)^{-1} \right) \\ \frac{N^2}{v'} \mathcal{P}_{poly}(\theta, N) + \frac{N^4}{v'^2} X \mathcal{P}^2_{poly}(\theta, N) \end{array} \right\} \times \tag{39}$$

$$\times | \int_{-\infty}^{t} d\tau e^{i\omega_{n+1}\tau} \langle V_L(\tau) \rangle_{\{n\}}|^2$$

S_{ST} represents the stimulated heterodyne detected signals including self-heterodyne detected techniques (pump-probe) and stimulated Hyper-Raman scattering. The remaining terms describe spontaneously generated signals. $S_{SP,incoh}$ is incoherent, phase insensitive and scales as $\sim N$ (e.g. multi-photon induced fluorescence). $S_{SP,coh,lr}$ describes the coherent response of all possible molecular pairs. Linear signals of this type are indistinguishable from the incident beam. Nonlinear signals include Hyper-Raman scattering and sum/difference frequency generation.

$S_{SP,coh,sr}$ is a short-range coherent spontaneous signal. Identical oriented polymer molecules give a directed phase matched signal. The degree of phase-matching depends on polymer size, internal structure and interaction between the polymers. Using the random-walk model we showed that the signal

contains two terms in the molecular density v'^{-1}.

We have further investigated nonlinear scattering from a non-ideal solution described by the osmotic pressure, density and fugacity. The signal is phase-insensitive and can be recast into an infinite series in the molecular density $\sum l\beta_l v^{-1}$. We discussed two limiting cases of ordinary and anomalous first order transitions and compared them to the hard sphere model. Such signals are both phase-insensitive and depend on the molecular density. We associated them with Rayleigh and Hyper-Rayleigh scattering.

Eqs. (35) provide a convenient starting point for the superoperator CTPL expansion of the nonlinear polarization based on the rules are given in Appendix B. We shall illustrate this for frequency domain spontaneous signals generated by two incoming classical fields: $\mathcal{E}_1 e^{-i\omega_1 t}$ and $\mathcal{E}_2 e^{-i\omega_2 t}$ in the vicinity of two-photon resonances $\omega_3 \approx \omega_1 + \omega_2$. The molecules are described by the three level ladder system: $\{\{|g\rangle, |g'\rangle\}, |e\rangle, |f\rangle\}$, shown in Fig. 4(B). The lowest manifold[1] contains the ground state $|g\rangle$ and higher level $|g'\rangle$.

The incoherent signal (37) gives rise to hyper-Raman and two-photon induced fluorescence which may be distinguished by including dephasing processes [1]. This goes beyond the scope of this presentation.

Since all incoming modes are classical, the frequency-domain signals can be recast in terms of nonlinear susceptibilities using the CTPL shown in Fig. 4(C1):

$$S_{HRAM,TPIF}(-\omega_3;\omega_2,\omega_1) = \tag{40}$$
$$= 2N\mathtt{Re}|\mathcal{E}_1|^2|\mathcal{E}_2|^2\chi^{(5)}_{LR---}(-\omega_3;\omega_3,-\omega_2,\omega_2,-\omega_1,\omega_1)$$

Here the susceptibility is recast in the mixed representation (L/R for the generated mode, and $+,-$ for the classical incoming modes [20]). It can be written in terms of the Green's function $G(\omega) = \hbar/(\hbar\omega - H_0 + i\hbar\gamma)^{-1}$ where

[1]The model also describes Brillouin scattering [30, 31]. That is the moving interference pattern, provided by the incoming pump fields and Stock shifted backward scattered generated wave, may create an acoustic wave. This, in turn, lifts the degeneracy of the molecular ground state and modifies the density dependent pre-factor for the short-range coherent signals. In some cases the acoustic wave may also reflect the incoming modes via spectral Bragg diffraction thus increasing the power of the generated signal. Brillouin scattering is a type of Raman scattering.

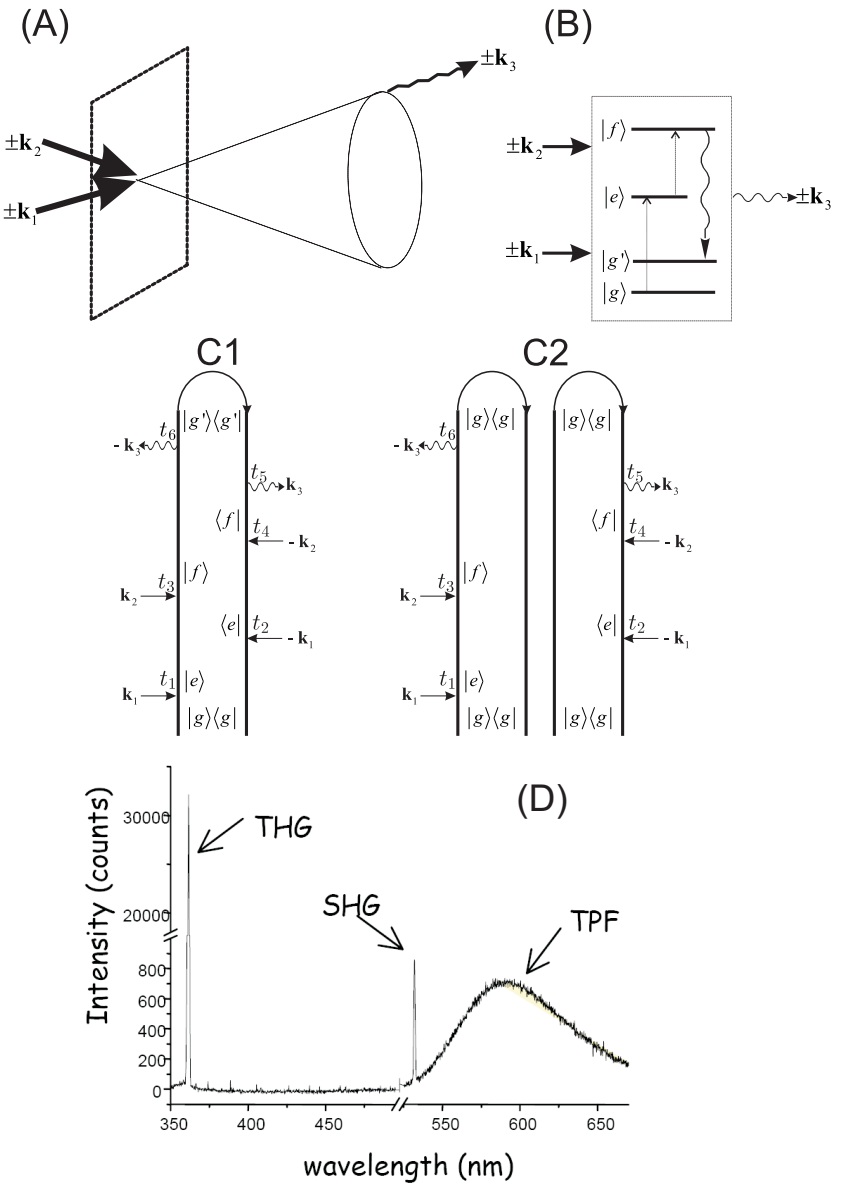

Figure 4: A three wave mixing process with two classical and one quantum modes: (A) phase-matching configuration; (B) molecular level scheme; CTPL for the incoherent Hyper-Raman and two-photon induced fluorescence (TPF) (C1) and long range coherent Homodyne detected sum frequency generation (SFG) as well as short range coherent Hyper-Rayleigh (C2). (D) measured spectra from PMMA polymers of oriented DCM [18].

γ is a dephasing rate:

$$\chi^{(5)}_{LR---}(-\omega_3;\omega_3,-\omega_2,\omega_2,-\omega_1,\omega_1) = \tag{41}$$
$$= \frac{i^5}{5!\hbar^5}\sum_p \langle g|VG^\dagger(\omega_g+\omega_1)VG^\dagger(\omega_g+\omega_1+\omega_2)V^\dagger\times$$
$$\times G^\dagger(\omega_g+\omega_1+\omega_2-\omega_3)VG(\omega_g+\omega_1+\omega_2)V^\dagger G(\omega_g+\omega_1)V^\dagger|g\rangle$$

Here p stands for permutations of the incoming field within each branch of the loop diagram. Expanding Eq.(41) in molecular energy levels $\hbar\omega_{eg},\hbar\omega_{ef},\hbar\omega_{fg}$ and the corresponding transition dipole moments $\mu_{eg},\mu_{ef},\mu_{fg}$ we finally obtain:

$$\chi^{(5)}_{LR---}(-\omega_3;\omega_3,-\omega_2,\omega_2,-\omega_1,\omega_1) = \tag{42}$$
$$= \frac{i^5}{5!\hbar^5}\sum_p\sum_{g,g'}\frac{|\mu_{eg}\mu_{ef}\mu_{fg'}|^2}{[(\omega_1-\omega_{eg})^2+\gamma^2]\,[\omega_1+\omega_2-\omega_{fg}+i\gamma]}\times$$
$$\times\frac{1}{[\omega_1+\omega_2-\omega_{fg'}-i\gamma]\,[\omega_1+\omega_2-\omega_3-\omega_{gg'}-i\gamma]}$$

The long-range coherent signal (38) for our model is a homodyne-detected sum frequency generation (SFG) [19, 32, 18]:

$$S_{SFG}(-\omega_3;\omega_2,\omega_1) = \tag{43}$$
$$= N(N-1)|\mathcal{E}_1|^2|\mathcal{E}_2|^2\mathcal{P}_{fluid}(\theta)\delta(\omega_3-\omega_2-\omega_1)\chi^{(2)}_{L--}(-\omega_3;\omega_2,\omega_1)|^2$$

This susceptibility can be calculated using the CTPL in Fig.4(C2):

$$\chi^{(2)}_{L--}(-\omega_3;\omega_2,\omega_1) = \sum_p\frac{i^2}{2!\hbar^2}\langle g|VG(\omega_g+\omega_1+\omega_2)V^\dagger G(\omega_g+\omega_1)V^\dagger|g\rangle =$$
$$= \sum_p\frac{i^2}{2!\hbar^2}\sum_g\frac{\mu_{ge}\mu_{ef}\mu_{fg}}{[\omega_1-\omega_{eg}+i\gamma]\,[\omega_1+\omega_2-\omega_{gf}=i\gamma]} \tag{44}$$

The short-range coherent signal (39) for our model is the density dependent hyper-Rayleigh (HRAY) scattering [33, 12, 13, 14]:

$$S_{HRAY}(-\omega_3;\omega_2,\omega_1) = \left\{\begin{array}{c} -\frac{N-1}{2}\mathtt{Re}\left(1-\left(1-\sum_{l\geq 1}l\beta_l v^{-l}\right)^{-1}\right) \\ \frac{N^2}{v'}\mathcal{P}_{poly}(\theta,N)+\frac{N^4}{v'^2}X\mathcal{P}^2_{poly}(\theta,N)\end{array}\right\}\times$$
$$\times|\mathcal{E}_1|^2|\mathcal{E}_2|^2|\delta(\omega_3-\omega_2-\omega_1)\chi^{(2)}_{L--}(-\omega_3;\omega_2,\omega_1)|^2 \tag{45}$$

In Fig. 4(D) we display an experimental spontaneously generated signal from a polymer solute [18]. The SFG signal has a sharp resonance, as expected from the delta function in Eq. (43), while the TPIF signal is broadened and covers the range of $\omega_{g',g}$ in accordance with Eq. (40). The hyper-Rayleigh signal (4) has the same resonance as SFG, since both are determined by the square of the second order susceptibility.

Note that all the signals discussed above are generated by classical incoming fields, and may be also calculated using semiclassical susceptibilities. However the present quantum treatment can predict signals generated by non-classical incoming modes [34, 35, 36]. Furthermore, even though we neglected the molecular orientational degrees of freedom, they play important role in distinguishing between SFG and HRAY processes. To take them into account we need to add a superscript to the transition dipole moment $\mu^i_{\alpha\beta}$ indicating its orientation with respect to the i-th component of the optical field. The intensity of (43) and (4) signals is then proportional to:

$$\langle(\mu^{i'}_{g'e'})^\star(\mu^{j'}_{e'f'})^\star(\mu^{k'}_{f'g'})^\star\mu^i_{ge}\mu^j_{ef}\mu^k_{fg}\rangle_{rav} \tag{46}$$

where primed and unprimed indices denote two different molecules in the molecular pair; $\langle\cdots\rangle_{rav}$ is rotational averaging [33]. For long-range coherent signals such as SFG, correlation between the two molecules in the pair is negligible and Eq. (46) can be factorized as: $|\langle\mu^i_{ge}\mu^j_{ef}\mu^k_{fg}\rangle_{rav}|^2$. In an isotropic media, this vanishes by symmetry [10, 37] leaving only the short-range coherent signals HRAY.

5 Acknowledgments

This work was supported by the National Science Foundation Grant CHE-0745892 and the Chemical sciences, Geosciences and Biosciences Division, Office of Basic Energy Sciences, Office of Sciences, U.S. Department of Energy. This support is gratefully acknowledged. We also wish to thank Professor Paul Berman most for useful discussions.

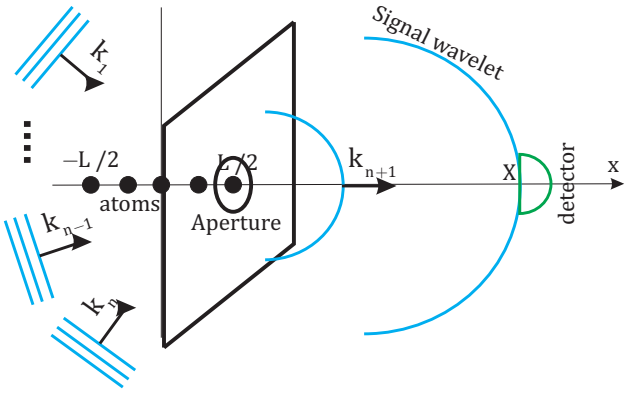

Figure 5: Semi-classical calculation of heterodyne detected incoherent nonlinear signals.

6 Appendixes

A Semiclassical vs. quantum field derivation of heterodyne-detected signals.

In this appendix we calculate the heterodyne detected incoherent nonlinear signal from a linear chain of molecules which interact with $n+1$ classical optical fields. The chain extends between $-L/2$ to $L/2$ along the x axis. The heterodyne detected signal is given by the electric field of the signal mode at $x = X$ far from the sample, as shown in Fig.5. We shall demonstrate equivalence of the semiclassical and quantum approaches.

Following Ref.[24] the semiclassical calculation will be divided into two steps. We first derive the electric field on the auxiliary object (aperture) via Maxwell's equations with the optical field driven by the nonlinear polarization of the atomic *primary* sources. Second, the aperture serves as the point *secondary* source of a spherical signal wave which is calculated with the propagator formalism.

For $k_{\{n\}}L \gg 1$, the sample can be treated as a continuous medium. The incoming waves create a nonlinear polarization wave along the sample:

$$P_{\{n\}}(x,t) = P_n(t) \exp\left(i\left(k_{\{n\}}x - \omega_{\{n\}}t\right)\right) \tag{47}$$

where $P_n(t)$ is slowly varying $|\frac{\partial}{\partial t}P_{\{n\}}(t)| \ll |\omega_{\{n\}}P_{\{n\}}(t)|$. This polarization is the primary source of the generated mode whose electric field is given by:

$$E_{n+1}(x,t) = \mathcal{E}_{n+1}(x,t)\exp\left(i(k_{n+1}x - \omega_{n+1}t)\right) \tag{48}$$

where $\mathcal{E}_{n+1}(t)$ is the slowly varying field amplitude (in space and time).

The electric field of the generated mode and the polarization induced by the incoming modes are connected by Maxwell's equations:

$$\left(\frac{\partial^2}{\partial x^2} + \left(\frac{k_{n+1}}{\omega_{n+1}}\right)^2 \frac{\partial^2}{\partial t^2}\right) E_{n+1}(x,t) = \tag{49}$$
$$= -\frac{4\pi}{c^2}\frac{\partial^2}{\partial t^2}P_{\{n\}}(x,t)$$

Substituting Eq. (47), (48) into (49) and using the slowly varying amplitude approximation for the generated and polarization we get:

$$ik_{n+1}\frac{\partial}{\partial x}\mathcal{E}_{n+1}(x,t) = \tag{50}$$
$$= -2\pi\frac{\omega_{\{n\}}^2}{c^2}P_{\{n\}}(t)\exp\left(i(\Delta k x - (\omega_{n+1} - \omega_{\{n\}})t)\right)$$

At the beginning of the illuminated region the amplitude of the generated mode vanishes $\mathcal{E}_{n+1}(-L/2,t) = 0$. Using this condition and integrating Eq. (50) over the sample range we obtain the generated mode at the aperture:

$$E_{n+1}(L/2,t) = -\frac{2\pi i\omega_{\{n\}}^2}{k_{n+1}c^2}P_{\{n\}}(t)L\texttt{sinc}(\Delta kL/2)\times \tag{51}$$
$$\times\exp\left(i(k_{n+1}L/2 - \omega_{n+1}t)\right)$$

The signal field is given by Fresnel diffraction from a point-like secondary source which correspond to a single Huygens wavelet:

$$E_{n+1}(X,t) = \tag{52}$$
$$= -\frac{i}{k_{n+1}X}E_{n+1}(L/2,t)\exp\left(i(X - L/2)k_{n+1}\right) =$$
$$= -\frac{2\pi}{Xn^2(\omega_n)}P_{\{n\}}(t)L\texttt{sinc}(\Delta kL/2)\times$$
$$\times\exp\left(i(k_{n+1}X - \omega_{n+1}t)\right)$$

Here $n(\omega_{n+1})$ is the refractive index of the sample and the $1/X$ factor accounts for the spherical nature of the Huygens wavelet. Unlike in the quantum calculations where the optical field is in the interaction picture and propagation effects are eliminated, E_{n+1} in Eq. (52) is the actual field at point X rather than the field generated at that point.

We now turn to the signal obtained from a quantum description of the field. Here each atom is the primary and only the source of the signal wave. $E_{n+1}(x,t)$ is the field *generated* at the point x since we are in the interaction picture where the free propagation is eliminated. The signal wave is now given by the interference from the Huygens wavelets constructed from $E_{n+1}(x,t)$ as in Eq. (3). Using Eq. (7) one can obtain equation of motion for the photon annihilation operator:

$$\frac{d}{dt}a_{n+1}(t) = i\left[H_{int}^{(n+1)}, a_{n+1}(t)\right] = \tag{53}$$
$$= i\int dx\sqrt{\frac{2\pi\omega_{n+1}}{\Omega_{n+1}}}\langle V(x,t)\rangle_{\{n\}}\exp\left(-i(k_{n+1}x-\omega_{n+1}t)\right)$$

We shall integrate Eq. (53) under the following conditions:

1. the expectation value of the polarization operator is given by Eq.(10);
2. initially the polarization $\langle V(x,-\infty)\rangle_{\{n\}}$ is zero;
3. the polarization has a slowly varying temporal amplitude:

$$\int_{-\infty}^{t}\langle V(\tau)\rangle_{\{n\}}d\tau = P_{\{n\}}(t)\frac{\exp\left(-i\omega_{\{n\}}t\right)}{-i\omega_{\{n\}}};$$

From Eq. (3) we obtain the signal optical field:

$$E_{n+1}(X,t) = \frac{-2N\pi\omega_{n+1}}{L\Omega_{n+1}\omega_{\{n\}}}\frac{(i(k_{n+1}X-\omega_{n+1}t))}{X}\times \tag{54}$$
$$\times P_{n+1}(t)\int_{-L/2}^{L/2}\exp\left(i\Delta kx\right)dx$$

Using the resonant condition $\omega_{n+1} - \omega_{\{n\}} \approx 0$, and Eq. (16), (17) we finally get:

$$E_{n+1}(X,t) = -\frac{2\pi N}{\Omega_{n+1} X} P_{\{n\}}(t) \mathtt{sinc}(\Delta k L/2) \times \\ \times \exp\left(i(k_{n+1}X - \omega_{n+1}t)\right) \tag{55}$$

By comparing Eq. (55) with (52) we find that the semiclassical and the quantum approaches give identical results, apart from the factors $L/n'(\omega_{n+1})$ vs. N/Ω_{n+1} which are model specific and arise from the single signal mode approximation. The heterodyne signal is obtained by treating the heterodyne wave as a spherical wave emitted by the aperture (which bring the Goui phase [24] factor $i/(k_{n+1}X)$): $\mathcal{E}_s(X,t) = i/(k_{n+1}X)\mathcal{E}_s(L,t)$ which brings up the Goui phase factor $i/(k_{n+1}X)$. Substituting the above equation along with Eq. (55)(or (52)) into the signal Eq. 4:

$$S_{HET} \sim \Im\langle V(\mathbf{r},t)\rangle_{\{n\}} \mathcal{E}^{\star}_{n+1}/X^2(\mathbf{r},t)$$

Formally we apply the Goui phase twice in Eq. 4 for propagating the signal and for the heterodyne part. This leads to an overall pre-factor of $1/(k_{n+1}X)^2$. the standard semiclassical procedure skips the propagation steps and uses Eq. (51) directly to yield $E_{n+1} \sim iP_n$.

B Generalized susceptibilities and their CTPL representation.

In this appendix we introduce the generalized susceptibilities used in the last section. These are based on the superoperator non-equilibrium Green's functions (SNGF's) [38, 39]. The n^{th} order SNGF's are defined as traces of time ordered products of such superoperators:

$$\langle \mathcal{T} A_+(t) \underbrace{A_+(t_n)\ldots A_+(t_{n-m+1})}_{m} \underbrace{A_-(t_{m-n})\ldots A_-(t_1)}_{n-m} \rangle$$

where $m = 0,\ldots,n$. The SNGF's may contain an arbitrary number of $+$ and $-$ superoperators. The chronologically last superoperator must be a "+" one, otherwise the SNGF vanishes.

The material $\mathbb{V}$ and optical $\mathbb{E}$ SNGF's are defined as:

$$\mathbb{V}^{(n)}_{L\nu_n\ldots\nu_1}(\tau,t_n,\ldots,t_1) = \langle \mathcal{T} V'_L(\tau)V'_{\nu_n}(t_n)\ldots V'_{\nu_1}(t_1)\rangle \tag{56}$$

$$\mathbb{E}^{(n)}_{\nu_n\ldots\nu_1}(t_n,\ldots,t_1) = \langle \mathcal{T} E'_{\bar{\nu}_n}(t_n)\ldots E'_{\bar{\nu}_1}(t_1)\rangle \tag{57}$$

where subscript ν is the superoperator index which depends on the representation; $V'_\nu = V_\nu + V^\dagger_\nu$ and the net field operators. SNGF's of the form $\mathbb{V}^{(m)}_{+\underbrace{-\ldots-}_{m}}$ give causal ordinary molecular response function of m^{th} order. The material SNGF of the form $\mathbb{V}^{(m)}_{+\underbrace{+\ldots+}_{m}}$ represent m^{th} moment of molecular fluctuations. The material SNGF of the form $\mathbb{V}^{(m)}_{+\underbrace{+\ldots+}_{m'}\underbrace{-\ldots-}_{m-m'}}$ indicates changes in m'^{th} moment of molecular fluctuations induced by $m-n$ light/matter interactions. In the other representation the material SNGF $\mathbb{V}^{(m)}_{L\underbrace{L\ldots L}_{n}\underbrace{R\ldots R}_{m-n}}$ represent a *Liouville space pathway* with $n+1$ interactions from the left (i.e. with the ket) and $m-n$ interactions from the right (i.e. with the bra).

The average material field in Eqs. (35)-(39) can be written in terms of the defined above SNGF's as:

$$\langle V_L(\tau)\rangle_{\{n\}} = \frac{i^n}{n!\hbar^n}\sum_{\nu_n}\ldots\sum_{\nu_1}\int_{-\infty}^{\infty} dt_n\ldots dt_1 \; \Theta(\tau)\mathbb{V}^{(n+1)}_{L\nu_n\ldots\nu_1}(\tau,t_n,\ldots,t_1)\times \mathbb{E}^{(n)}_{\bar{\nu}_n\ldots\bar{\nu}_1}(t_n,\ldots,t_1) \tag{58}$$

where $t_n,\ldots,t_1$ are the incoming modes light/matter interaction times. The factor $\Theta(\tau)=\prod_{i=1}^{n}\theta(\tau-t_i)$ guarantees that the τ is the last light-matter interaction with the detected mode which has been taken care of separately. The indices $\bar{\nu}_j$ are the conjugates to ν_j and are defined as follows: the conjugate of $+$ is $-$. However the conjugate of L is L and R is R. Eq. (58) implies

that is the excitations in the material are caused by fluctuations in the optical field and vice versa. Here we use a mixed representation in order to separate classical incoming ($\pm$ representation) and quantum detected (L, R representation) optical modes.

Eqs. (40), (43), (4) were obtained by recasting material SNGF's in Eq. (58) into the form of generalized susceptibilities. These are formally defined as in the frequency domain by performing a multiple Fourier transform:

$$\chi^{(n)}_{L\nu_n\ldots\nu_1}(-\omega_{n+1};\omega_n,\ldots,\omega_1) = \int_{-\infty}^{\infty} d\tau\ldots dt_1\Theta(\tau)e^{i(\omega_n t_n+\ldots+\omega_1 t_1)} \delta(-\omega_{n+1}+\omega_n+\ldots+\omega_1)\mathbb{V}^{(n)}_{L\nu_n\ldots\nu_1}(\tau,t_n,\ldots,t_1) \tag{59}$$

The SNGF $\chi^{(n)}_{+\underbrace{-\ldots-}_{n}}(-\omega_{n+1};\omega_n,\ldots,\omega_1)$ (with one + and the rest $-$ indices) are the n^{th} order nonlinear susceptibilities or causal response functions. Others can be interpreted similarly to their time domain counterparts (56).

The generalized susceptibilities written in terms of L, R superoperators, can be represented by close-time path loop (CTPL) diagrams introduced by Schwinger-Keldysh many body theory. The following rules are used to construct these diagrams [21, 11]:

1. Time runs along the loop clockwise from bottom left to bottom right.

2. The left branch of the loop represents the "ket", the right represents the "bra".

3. Each interaction with a field mode is represented by an arrow line on either the right (R-operators) or the left (L-operators).

4. The field is marked by dressing the lines with arrows, where an arrow pointing to the right (left) represents the field annihilation (creation) operator $E_\alpha(t)$ ($E^\dagger_\alpha(t)$).

5. Within the RWA, each interaction with the field annihilates the photon $E_\alpha(t)$ and is accompanied by applying the operator $V^\dagger_\alpha(t)$, which leads to excitation of the state represented by ket and dexcitating of the state represented by the bra, respectively. Arrows pointing "inwards" (i.e. pointing to the right on the ket and to the left on the bra) consequently

cause absorption of a photon by exciting the system, whereas arrows pointing "outwards" (i.e. pointing to the left on the bra and to the right on the ket) represent dexcitating the system by photon emission.

6. The observation time t, is fixed and is always the last. As a convention, it is chosen to occur from the left. This can always be achieved by a reflection of all interactions through the center line between the ket and the bra, which corresponds to taking the complex conjugate of the original correlation function.

7. The loop translates into an alternating product of interactions (arrows) and periods of free evolutions (vertical solid lines) along the loop.

8. Since the loop time goes clockwise along the loop, periods of free evolution on the left branch amount to propagating forward in real time with the propagator give by the retarded Green's function G. Whereas evolution on the right branch corresponds to backward propagation (advanced Green's function $G^{\dagger}$).

9. The frequency arguments of the various propagators are cumulative, i.e. they are given by the sum of all "earlier" interactions along the loop. Additionally, the ground state frequency is added to all arguments of the propagators.

10. The Fourier transform of the time-domain propagators adds an additional factor of $i(-i)$ for each retarded (advanced) propagator.

11. The overall sign of the SNGF is given by $(-1)^{N_R}$, where N_R stands for the number of R superoperators.

References

[1] S. Mukamel. *Principles of nonlinear optical spectroscopy.* Oxford University Press New York, 1995.

[2] S. Mukamel and E. Hanamura. Four-wave mixing using partially coherent fields in systems with spatial correlations. *Phys. Rev. A*, 33:1099, 1986.

[3] D.L. Andrews and P. Allcock. *Optical harmonics in molecular systems*. Wiley-VCH Weinheim, 2002.

[4] R.J. Glauber. *Quantum Theory of Optical Coherence: Selected Papers and Lectures*. Wiley-VCH, 2007.

[5] MO Scully and MS Zubairy. *Quantum Optics*. Cambridge University Press, 1997.

[6] N. Bloembergen. *Nonlinear Optics*. World Scientific, 1996.

[7] W. Denk, JH Strickler, and WW Webb. Two-photon laser scanning fluorescence microscopy. *Science,*, 248(4951):73, 1990.

[8] J. Mertz. Nonlinear microscopy: new techniques and applications. *Current opinion in neurobiology*, 14(5):610–616, 2004.

[9] PD Maker. Spectral broadening of elastic second-harmonic light scattering in liquids. *Phys. Rev. A,*, 1(3):923, 1970.

[10] RW Terhune, PD Maker, and CM Savage. Measurements of nonlinear light scattering. *Physical Review Letters*, 14(17):681–684, 1965.

[11] C.A. Marx, U. Harbola, and S. Mukamel. Nonlinear optical spectroscopy of single, few, and many molecules: Nonequilibrium Greens function QED approach. *Phys. Rev. A,*, 77(2):22110, 2008.

[12] K. Clays and A. Persoons. Hyper-Rayleigh scattering in solution. *Phys. Rev. Lett.,*, 66(23):2980, 1991.

[13] G. Olbrechts, T. Munters, K. Clays, A. Persoons, O.K. Kim, and L.S. Choi. High-frequency demodulation of multi-photon fluorescence in hyper-Rayleigh scattering. *Optical Materials*, 12(2):221, 1999.

[14] M.C. Flipse, R. de Jonge, R.H. Woudenberg, A.W. Marsman, C.A. van Walree, and L.W. Jenneskens. The determination of first hyperpolarizabilities β using hyper-Rayleigh scattering: a caveat. *Chemical Physics Letters*, 245(2-3):297–303, 1995.

[15] A.S. Ranjini, P.K. Das, and P. Balaram. Binding Constant Measurement by Hyper-Rayleigh Scattering: Bilirubin- Human Serum Albumin Binding as a Case Study. *J. Phys. Chem. B*, 109:5950, 2005.

[16] S.J. Cyvin, J.E. Rauch, and J.C. Decius. Theory of hyper-Raman effects (nonlinear inelastic light scattering): selection rules and depolarization ratios for the second-order polarizability. *The Journal of Chemical Physics*, 43:4083, 1965.

[17] J.H. Christie and D.J. Lockwood. Selection Rules for Three-and Four-Photon Raman Interactions. *The Journal of Chemical Physics*, 54:1141, 1971.

[18] V. Le Floc'h, S. Brasselet, J.F. Roch, and J. Zyss. Monitoring of orientation in molecular ensembles by polarization sensitive nonlinear microscopy. *J. Phys. Chem. B*, 107(45):12403, 2003.

[19] M. Strupler, A.M. Pena, M. Hernest, P.L. Tharaux, J.L. Martin, E. Beaurepaire, and M.C. Schanne-Klein. Second harmonic imaging and scoring of collagen in fibrotic tissues. *Optics Express*, 15(7):4054–4065, 2007.

[20] O. Roslyak and S. Mukamel. A unified description of sum frequency generation, parametric down conversion and two-photon fluorescence. *Molecular Physics*, 107(3):265, 2009.

[21] O. Roslyak, C.A. Marx, and S. Mukamel. Generalized Kramers-Heisenberg expressions for stimulated Raman scattering and two-photon absorption. *Physical Review A*, 79(6):63827, 2009.

[22] B.H. Zimm. Molecular theory of the scattering of light in fluids. *The Journal of Chemical Physics*, 13:141, 1945.

[23] S. Mukamel. Solvation Effects on Four-Wave Mixing and Spontaneous Raman and Fluorescence Lineshapes of Polyatomic Molecules. *Adv. Chem. Phys.*, 70:165, 1988.

[24] N. Mertz. *Introduction to optical microscopy*. Roberts & Co, 2009.

[25] B.H. Zimm. The scattering of light and the radial distribution function of high polymer solutions. *The Journal of Chemical Physics*, 16:1093, 1948.

[26] B.H. Zimm. Application of the methods of molecular distribution to solutions of large molecules. *The Journal of Chemical Physics*, 14:164, 1946.

[27] J.E. Mayer and E. Montroll. Molecular distribution. *The Journal of Chemical Physics*, 9:2, 1941.

[28] J.E. Mayer and SF Harrison. Statistical mechanics of condensing systems. III. *The Journal of Chemical Physics*, 6:87, 1938.

[29] J.E. Mayer. Contribution to Statistical Mechanics. *The Journal of Chemical Physics*, 10:629, 1942.

[30] K. Brown, A.W. Brown, and B.G. Colpitts. Characterization of optical fibers for optimization of a Brillouin scattering based fiber optic sensor. *Optical Fiber Technology*, 11(2):131, 2005.

[31] Q. Lin, O.J. Painter, and G.P. Agrawal. Nonlinear optical phenomena in silicon waveguides: modeling and applications. *Optics Express*, 15(25):16604–16644, 2007.

[32] K. Komorowska, S. Brasselet, G. Dutier, I. Ledoux, J. Zyss, L. Poulsen, M. Jazdzyk, H.J. Egelhaaf, J. Gierschner, and M. Hanack. Nanometric scale investigation of the nonlinear efficiency of perhydrotriphenylene inclusion compounds. *Chemical Physics*, 318(1):12, 2005.

[33] K. Clays, E. Hendrickx, M. Triest, T. Verbiest, A. Persoons, C. Dehu, and J.L. Bredas. Nonlinear optical properties of proteins measured by hyper-Rayleigh scattering in solution. *Science*, 262(5138):1419, 1993.

[34] O. Roslyak and S. Mukamel. Photon entanglement signatures in difference-frequency-generation. *Optics express*, 17(2):1093–1106, 2009.

[35] O. Roslyak, C.A. Marx, and S. Mukamel. Nonlinear spectroscopy with entangled photons: Manipulating quantum pathways of matter. *Physical Review A*, 79(3):33832, 2009.

[36] O. Roslyak and S. Mukamel. Multidimensional pump-probe spectroscopy with entangled twin-photon states. *Physical Review A*, 79(6):63409, 2009.

[37] M. Kauranen, C. Boutton, T. Verbiest, M. N. Teerenstra, K. Clays, A. J. Schouten, R. J. M. Nolte, and A. Persoons. Supramolecular second-order nonlinearity of polymers with orientationally correlated chromophores. *Science*, 270:966, 1995.

[38] Adam E. Cohen and Shaul Mukamel. Resonant enhancement and dissipation in nonequilibrium van der waals forces. *Phys. Rev. Lett.*, 91:233202, 2003.

[39] Upendra Harbola and Shaul Mukamel. Superoperator nonequilibrium greens function theory of many-body systems; application to charge transfer and transport in open junctions. *Physics Reports*, 465:191, 2008.